Author(s): Kumar, D.; Dickel, T.; Zadvornaya, A.; Beliuskina, O.; Kankainen, A.; Constantin, P.; Purushothaman, S.; Spataru, A.; Stryjczyk, M.; Al Ayoubi, L.; Brunet, M.; Canete, L.; Delafosse, C.; de Groote, R.P.; de Roubin, A.; Eronen, T.; Ge, Z.; Gins, W.; Hornung, C.; Hukkanen, M.; Illana, A.; Jokinen, A.; Kahl, D.; Kindler, B.; Lommel, B.; Mardor, I.; Moore, I.D.; Nesterenko, D.A.; Nichita, D.; Nikas, S.; Ortiz-Cortes,

Title: First investigation on the isomeric ratio in multinucleon transfer reactions : Entrance channel effects on the spin distribution

Year: 2024

Version: Published version

Phys. Lett. B 853 (2024) 138654

Contents lists available at ScienceDirect

Physics Letters B

journal homepage: www.elsevier.com/locate/physletb

Letter

First investigation on the isomeric ratio in multinucleon transfer reactions: Entrance channel effects on the spin distribution

D. Kumar [a,*], T. Dickel [a,b], A. Zadvornaya [b,c,d], O. Beliuskina [c], A. Kankainen [c], P. Constantin [e], S. Purushothaman [a], A. Spataru [e], M. Stryjczyk [c], L. Al Ayoubi [c,f], M. Brunet [g], L. Canete [c], C. Delafosse [c,f], R.P. de Groote [c,h], A. de Roubin [c], T. Eronen [c], Z. Ge [a,c], W. Gins [c], C. Hornung [a], M. Hukkanen [c,i], A. Illana [c,j], A. Jokinen [c], D. Kahl [e,k], B. Kindler [a], B. Lommel [a], I. Mardor [l,m], I.D. Moore [c], D.A. Nesterenko [c], D. Nichita [e], S. Nikas [c], A. Ortiz-Cortes [c], H. Penttilä [c], Zs. Podolyák [g], I. Pohjalainen [c], A. Raggio [c], M. Reponen [c], S. Rinta-Antila [c], J. Romero [c,n], J. Saren [c], M. Vilen [c], V. Virtanen [c], A. Weaver [o], J. Winfield [a,l]

[a] GSI Helmholtzzentrum für Schwerionenforschung GmbH, Darmstadt, 64291, Germany
[b] II. Physikalisches Institut, Justus-Liebig-Universität Gießen, Gießen, 35392, Germany
[c] University of Jyväskylä, Department of Physics, Accelerator laboratory, P.O. Box 35(YFL) FI-40014 University of Jyväskylä, Finland
[d] Helmholtz Research Academy Hesse for FAIR (HFHF), GSI Helmholtz Center for Heavy Ion Research, Campus Gießen, 35392 Gießen, Germany
[e] Extreme Light Infrastructure-Nuclear Physics, Horia Hulubei National Institute for R&D in Physics and Nuclear Engineering, Măgurele, 077125, Romania
[f] Université Paris Saclay, CNRS/IN2P3, IJCLab, 91405, Orsay, France
[g] Department of Physics, University of Surrey, Guildford, GU2 7XH, United Kingdom
[h] KU Leuven, Instituut voor Kern- en Stralingsfysica, Leuven, B-3001, Belgium
[i] Université de Bordeaux, CNRS/IN2P3, LP2I Bordeaux, UMR 5797, F-33170, Gradignan, France
[j] Grupo de Física Nuclear & IPARCOS, Universidad Complutense de Madrid, CEI Moncloa, 28040, Madrid, Spain
[k] Facility for Rare Isotope Beams, Michigan State University, 640 South Shaw Lane, East Lansing, MI 48824, USA
[l] Tel Aviv University, Tel Aviv,6997801, Israel
[m] Soreq Nuclear Research Center, Yavne, 8180000, Israel
[n] Oliver Lodge Laboratory, University of Liverpool, Liverpool, L69 7ZE, United Kingdom
[o] School of Computing, Engineering and Mathematics, University of Brighton, Brighton, BN2 4GJ, United Kingdom

ARTICLE INFO

Editor: H. Gao

Keywords:
Multinucleon transfer (MNT) reaction
Isomeric-to-ground state ratio (IR)
Gas-filled stopping cells
α-spectra

ABSTRACT

The multinucleon transfer (MNT) reaction approach was successfully employed for the first time to measure the isomeric ratios (IRs) of ^{211}Po isomer ($25/2^+$) and its ground state ($9/2^+$) at the IGISOL facility using a 945 MeV ^{136}Xe beam impinged on ^{209}Bi and ^{nat}Pb targets. The dominant production of isomers compared to the corresponding ground states was consistently revealed in the α-decay spectra. Deduced IR of ^{211}Po populated through the ^{136}Xe+^{nat}Pb reaction was found to have an enhancement of ≈1.8-times than that observed for the ^{136}Xe+^{209}Bi. State-of-the-art Langevin-type model calculations have been utilized to estimate the spin distribution of an MNT residue. The computations qualitatively corroborate with the considerable increase in the IRs of ^{211}Po produced from ^{136}Xe+^{nat}Pb compared to ^{136}Xe+^{209}Bi. Theoretical investigations indicate a weak dependence of target spin on the IRs. The enhancement of the ^{211}Po isomer in the ^{136}Xe+^{nat}Pb over ^{136}Xe+^{209}Bi can be attributed to the different proton (p)-transfer production routes. Estimations demonstrate an increment in the angular momentum transfer, favorable for isomer production, with increasing projectile energy. Comparative analysis reveals the two entrance channel parameters, projectile mass and p-transfer channels, strongly influencing the population of the high-spin isomer of ^{211}Po ($25/2^+$). This letter reports the first experimental and theoretical study on the IRs of nuclei formed from two different p-transfer channels via two independent MNT reactions.

* Corresponding author.
E-mail addresses: De.Kumar@gsi.de, dekumar.gsi@gmail.com (D. Kumar).
[1] Deceased.

https://doi.org/10.1016/j.physletb.2024.138654
Received 15 January 2024; Received in revised form 27 March 2024; Accepted 14 April 2024
Available online 18 April 2024

1. Introduction

The crux of exploring nuclear reaction and structural properties of heavy neutron-rich nuclei is to grasp an understanding of the evolution of shell structure far from the valley of β-stability, which in turn is crucial for the astrophysical rapid neutron capture process (r-process) [1–3]. Of all the nuclear properties, experimental data on isomeric ratios (IRs) is essential to comprehend the spin distributions, which eventually affect the population of isomers. Knowledge of the proper production routes of exotic neutron-rich isomers is vital for studying nuclear structural aspects like half-lives, spins, decay paths, etc., which play a prominent role in driving the r-process pathways [4,5]. The impact of studying IRs is also relevant for mass measurements, where unresolved isomers can lead to uncertainties. Investigating the optimum production routes for heavy neutron-rich isomers ultimately encompasses a broader motive from nuclear reactions to the nuclear structural study, which profoundly impacts the isomer studies of superheavy nuclei as well [6,7]. Furthermore, nuclear isomers can be exploited for application purposes such as the flourishing branch of nuclear medicine, energy storage, etc. [8–13].

The MNT reaction approach has emerged as a pragmatic pathway for accessing the heavy neutron-rich uncharted terrain of the nuclear chart spanning from the rare-earth region to the "Island of Stability" [14–16]. The MNT fragments, heavier than fission-like fragments, are extended across quasi-elastic (QE) and deep-inelastic collision (DIC) regimes [16–20]. The promising outcomes of advanced MNT models at neutron shell closures, particularly $N = 126$, have steered many experiments towards using ^{136}Xe+^{208}Pb, ^{136}Xe+^{198}Pt, ^{204}Hg+^{208}Pb, and ^{64}Ni+^{207,208}Pb reactions at above barrier energies during the last two decades [21–40]. However, none of these experiments were focused on studies of spin distribution of MNT fragments. To date, comprehensive studies of MNT reaction properties for limited target-projectile systems have been carried out using in-flight electromagnetic separators such as VAMOS++ along with EXOGAM, AGATA, and CATLIFE at GANIL [31–34], PRISMA coupled to AGATA and CLARA at INFN LNL in Legnaro [16,41–43], MAGNEX at INFN-LNS in Catania [44,45], and SHIP velocity filter at GSI [3,39]; except for decay/in-beam γ-ray spectroscopy work performed using the Gammasphere facility at ANL [35–38]. However, the discovery of any unknown nuclei would be precluded in any of those methods, in which the identification of nuclei can only be determined by known γ- or α-decay patterns. In addition, similar studies were also carried out using the CORSET setup at Dubna [30] and a ΔE–E Si-detector telescope together with four MWPCs at JAEA [46].

The strenuous attempt to overcome experimental challenges in the production, separation, and identification of heavy MNT fragments is still being continued across various nuclear laboratories around the globe [47–49]. Several ion-catcher setups have been commissioning in recent years to span a broader coverage of the angular distribution of MNT fragments, such as the MNT gas cell at IGISOL [50,51], FRS ion-catcher (IC) with INCREASE at GSI [49,52], $N = 126$ factory at ANL [53], and NEXT at Groningen [54]. The KISS experiment at RIKEN has recently led to a breakthrough by measuring an unknown uranium isotope ^{241}U using ^{238}U+^{198}Pt in addition to many neutron-rich projectile-like fragments thermalized within a gas cell [55]. Moreover, spectroscopic investigations on several target-like fragments (TLFs) of Os-Pt isotopes in many experiments of ^{136}Xe+^{198}Pt have built up promising prospects for the MNT methodology to produce many more undiscovered nuclei [56–59]. In this endeavor, a comprehensive and systematic program for MNT reactions using different types of newly developed MNT-ion catchers at the IGISOL (JYFL) and FRS-IC (GSI) facilities has been initiated in the interest of addressing both aspects of nuclear features: (i) to measure (relative) production cross-sections and IRs in order to benchmark the state-of-the-art MNT models; and (ii) to produce neutron-rich exotic isotopes and isomers for nuclear structural studies and mass measurements [49,51].

State-of-the-art MNT models differ by orders of magnitude for the nuclei produced by transferring a few nucleons from the target/projectile (e.g., $\Delta Z \geq 2$) or for symmetric target-projectile systems [35–38]. This generates urgent interest in validating these models by comparing them with the reaction data of different forms. This letter reports the first measurements of IRs populated via the MNT reactions. The IR manifests the characteristics of the spin distribution of MNT fragments. Moreover, computations of the spin distribution of the MNT fragment are performed for the first time using improved state-of-the-art Langevin-type model calculations and benchmarked by comparing it with the measured IRs.

2. Experimental study

A series of experiments were performed during the commissioning of dedicated MNT gas cells with the aim of accessing neutron-rich exotic nuclei utilizing the MNT approach at the Ion-Guide Isotope Separator On-Line (IGISOL) facility of the JYFL Accelerator Laboratory, University of Jyväskylä, Finland [60,61]. The TLFs were produced using a 945±9 MeV ^{136}Xe beam delivered by the K-130 heavy-ion cyclotron. A schematic diagram of experimental setups inside the target chamber consists of the target, the gas cell, the beam dump, the sextupole ion guide (SPIG), and the extractor electrodes, as shown in Fig. 1. Three configurations of the gas cells were tested in different experiments [50]. The primary beam was stopped within a graphite beam-dump mounted either in front of the gas cell (modified HIGISOL and MNT gas cell in A-configuration) or after the gas cell (MNT gas cell in B-configuration) [50].

In experiments I, II, and IV (see Table 1), the primary beam was allowed to incident on a ^{209}Bi target having a thickness of ≈5.1 mg/cm^2. The projectile energy loss within the target was estimated as 945–792 MeV using the SRIM code [62], which leads to a mid-target energy 868±77 MeV or equivalently, an energy above the Coulomb barrier, $E/V_B = 1.23 \pm 0.11$. Similarly, in experiment III, the beam impinged on a ≈6 mg/cm^2 ^{nat}Pb target. The projectile energy loss was estimated as 945–765 MeV, which results in a mid-target energy 855±90 MeV or equivalently, $E/V_B = 1.21 \pm 0.12$.

The energetic MNT fragments produced from the target were passed through the gas cell's nickel (Ni) or havar window. The fragments were stopped within the He buffer gas inside the gas cell. The gas flow subsequently extracted the thermalized ions from the gas cell, from which they were guided through a radiofrequency SPIG and extractor electrode system towards the mass separator [63]. The target chamber was kept at +30 kV. The extracted ions were gradually accelerated towards the grounded electrostatic switchyard (SW), with typical voltage differences shown in Fig. 1 and mass separated using a dipole magnet having a mass resolving power ($M/\Delta M$), $R \approx 300$, placed before the SW. Finally, in-beam α-decay spectra were measured using a Silicon (Si) detector mounted at the SW.

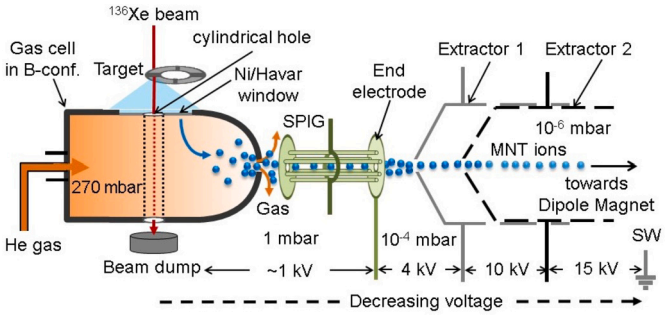

Fig. 1. A schematic diagram of the experimental arrangements consisting of a target, the MNT gas cell in B-configuration [50], the beam dump, He gas flow, the sextupole ion guide (SPIG), and the extractor electrodes [63].

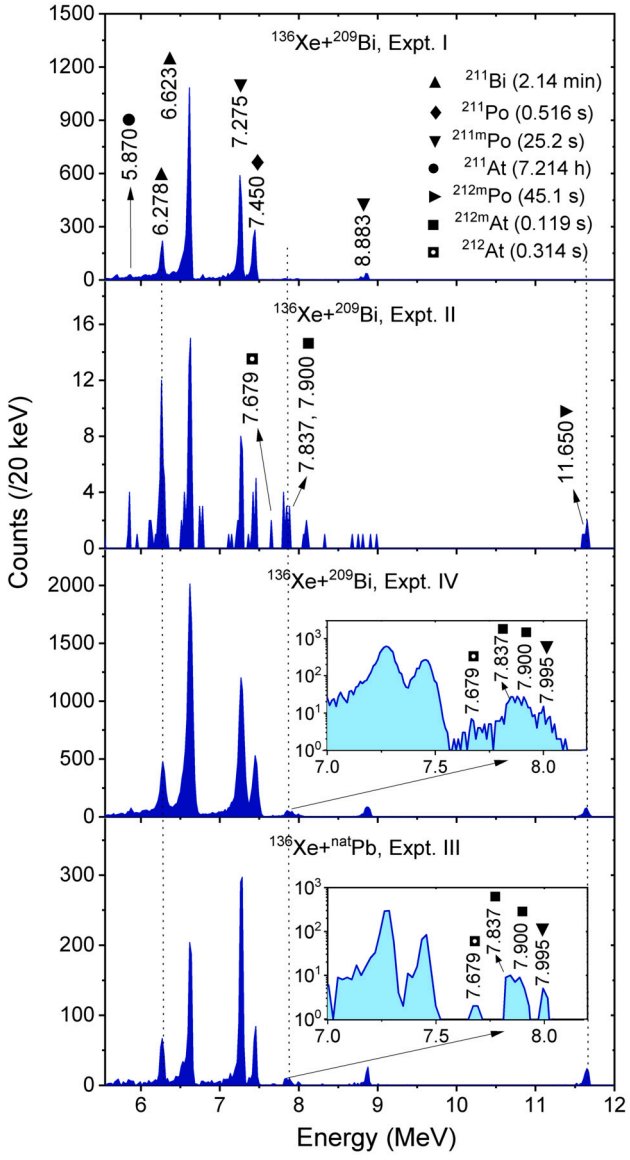

Fig. 2. Characteristics α-decay spectra of TLFs measured in three independent experiments using ^{136}Xe+ ^{209}Bi at E/V$_B$ = 1.23±0.11 and one with ^{136}Xe+ ^{nat}Pb at E/V$_B$ = 1.21±0.12 for different gas cell configurations.

The characteristic α-decay peaks of ^{211}Bi, ^{211m}Po, ^{211}Po, and ^{212m}Po were identified in addition to a minute amount of ^{211}At, ^{212m}At, and ^{212}At, as shown in Fig. 2. The dipole magnet was set at mass, A = 211. However, the presence of α-decay peaks from the neighboring mass, A = 212, is due to a limited resolving power of the dipole magnet. The α-spectrum of Expt. II, collected before the magnet, also reveals this when compared with the other experimental spectra (Expt. I, III, and IV) taken at SW. The Expt II, compared to others, shows a more significant production of mass (A) 212 nuclei (i.e., ^{212}At, ^{212m}At, ^{212m}Po) relative to the mass (A) 211 nuclei. As evident from Fig. 2, the relative production of different α-emitting MNT fragments is found to be consistent across spectra, with ^{211}Bi as the dominant peak in all three measurements of the ^{136}Xe+ ^{209}Bi reaction. However, the most intense α-decay peak of ^{211m}Po (i.e., 7275 keV) was dominantly observed in the ^{136}Xe+ ^{nat}Pb reaction among all other peaks. It is important to mention that the broader angular distributions of MNT fragments would result in a wider spreading of thermalized MNT ions inside the gas cell [22], which would cause a significant variation in extraction time, i.e., transport time from within the gas cell to the SW (typically 100 ms). This leads to a larger uncertainty in the yields of ^{212m}At and ^{212}At in addition to the lower statistics; thereby, the estimation of IR of ^{212}At is excluded.

The IR of ^{211}Po was scrutinized against various experimental conditions: (i) different beam intensities, I (pnA); (ii) angular coverage of the gas cell window; (iii) He gas pressure within the gas cell, P (mbar); tabulated in Table 1. Additionally, the carbon (C) catcher foils before the Si detector, the slit width opening at the electrostatic SW, and the thickness of the gas cell window, including the utilized material, would also affect the product yields and are, therefore, enlisted in Table 1. The isomeric yield (i.e., isomer-to-ground state) ratio (IYR) of the ^{211}Po was deduced and normalized with the corresponding α-peak intensities. Therefore, the deduced IYR would be equivalent to the isomeric cross-section ratio (ICR), independent of experimental parameters, as manifested in Table 1. Hence, this letter refers to IYR or ICR as IR.

3. Computations of spin distributions and IRs

A multidimensional dynamical approach based on Langevin equations has been adopted to examine the measured data. The dynamical approach has adequately reproduced the mass, charge, energy, and angular distributions of the MNT-induced products for most of the studied reactions so far [21–24]. The model has been extended to provide information about the spin distribution, thereby enabling the theoretical study of the spin distribution of MNT fragments for the first time. The calculation of IR of a nuclide produced via the MNT reaction can be conceptualized into two steps: (i) estimation of the spin distribution of an MNT fragment, and (ii) feeding of isomeric and ground states from the spin distribution. In the first step, the total angular momentum distribution was estimated by folding the orbital angular momentum with the non-zero intrinsic spin of the target. Moreover, the exchange of angular momentum due to the transfer of nucleons from projectile to target is necessary for the population of trans-target products, e.g., ^{211}Po, ^{211}Bi, etc. This was implemented as the sequential transfer of the nucleons. The spin of an excited MNT fragment is also affected by the evaporation of nucleons, although this effect was not included.

In the second step, the IR of ^{211}Po has been calculated by splitting the spin distribution into two parts: the lower spin distribution region is assumed to feed the ground-state ($9/2^+$), and the higher-spin distribution to the isomeric state ($25/2^+$). The spread in the spin distribution can be anticipated due to the evaporation of nucleons and the cascade of γ-decays from the MNT fragments. To account for these effects, an empirical systematic approach was applied for the calculation of IR using equation (1), consisting of an effective angular momentum cutoff J_{eff}, and a spreading parameter Δ [64],

$$IR = \frac{\sum_J Y_J^{(\text{m})}}{\sum_J Y_J^{(\text{g})}}, \tag{1}$$

$$Y_J^{(\text{g})} = \frac{Y_J^{(\text{theory})}}{(1 + exp\frac{(J_{\text{eff}} - J)}{\Delta})}; Y_J^{(\text{m})} = \frac{Y_J^{(\text{theory})}}{(1 + exp\frac{(J - J_{\text{eff}})}{\Delta})}. \tag{2}$$

The $Y_J^{(\text{theory})}$, $Y_J^{(\text{g})}$, and $Y_J^{(\text{m})}$ correspond to the theoretical estimation, the ground-state, and the isomeric state of spin distribution of an MNT fragment, respectively. In the calculations, we assumed Δ = 0.5, which is justified to account for the angular momentum carried away by the neutrons and γ-rays [64–66].

In this work, the spin distribution of ^{211}Po was calculated for both reactions: ^{136}Xe+ ^{209}Bi at E/V$_B$ = 1.12, 1.26, and 1.33; and ^{136}Xe+ ^{nat}Pb at E/V$_B$ = 1.13, 1.27, and 1.34 [67]. Fig. 3(a) demonstrates the variation in the spin distributions of ^{211}Po for the two energies in both cases. It is found that the most probable value of spin distributions at near barrier energy (*i.e.*, E/V$_B$ = 1.12 and 1.13) is lower compared to the spin of the isomeric state of ^{211}Po ($25/2^+$) as marked using a vertical line. However, the spin distributions for higher projectile energy (at E/V$_B$ = 1.33 and 1.34) are significantly different for both reactions. The most probable value of the spin distribution obtained from ^{136}Xe+ ^{nat}Pb

Table 1
Measured yields (Y) of ^{211m}Po, ^{211}Po, and the subsequently deduced isomeric ratio (IR) of ^{211}Po for a 945±9 MeV $^{136}Xe^{31+}$ beam at different experimental conditions: intensity (I) of the beam, angular coverage (Ang. cov.) of the gas-cell window (±1°–3° uncertainty), pressure (P) of the He gas, thickness of carbon (C) foil placed before the Si detector, and slit width opening at the entrance to the electrostatic switchyard. The thickness of the entrance window of the gas cell was 4.3 mg/cm^2 Havar used in Expt. I-II, whereas 4.8 mg/cm^2 Ni was used in Expt. III-IV.

Expt. (Gas cell type)	Month/Year (Target)	I (pnA)	Ang. cov. (deg. (°))	P (mbar)	C foil (μg/cm^2)	width (mm)	$Y_{^{211m}Po}$ (1/min)	$Y_{^{211}Po}$ (1/min)	IR of ^{211}Po
Expt. I	06/2019	10	29–49	300	-	7	8.5 ± 0.2	4.0 ± 0.2	2.3 ± 0.2
(Modified HIGISOL)	(^{209}Bi)	10	29–49	300	-	7	8.9 ± 0.2	4.1 ± 0.2	2.4 ± 0.2
Expt. II	08/2019	20	29–49	300	-	10	1.4 ± 0.2	0.8 ± 0.1	1.9 ± 0.5
(Modified HIGISOL)	(^{209}Bi)	20	18–42	300	-	10	0.7 ± 0.1	0.4 ± 0.1	1.8 ± 0.7
Expt. III	03/2021	30	27–60	235	-	7.5	8.9 ± 0.3	2.0 ± 0.2	4.8 ± 0.5
(MNT gas cell	(^{nat}Pb)	30	27–60	250	195	7.5	6.4 ± 0.3	1.7 ± 0.2	4.0 ± 0.6
A-configuration)		20	45–65	220	190	7.5	2.0 ± 0.1	0.5 ± 0.1	4.7 ± 1.0
		20	27–60	220	190	7.5	4.9 ± 0.2	1.2 ± 0.1	4.4 ± 0.6
		30	27–60	270	195	7.5	5.4 ± 0.2	1.3 ± 0.1	4.4 ± 0.6
Expt. IV	11/2021	30	20–55	265	-	10	75.4 ± 1.5	32.4 ± 1.0	2.5 ± 0.1
(MNT gas cell	(^{209}Bi)	20	17–51	260	205	10	28.4 ± 1.1	11.8 ± 0.7	2.6 ± 0.2
B-configuration)		28	17–51	262	-	10	73.8 ± 1.6	29.3 ± 1.0	2.7 ± 0.2
		20	14–48	262	195	10	42.2 ± 1.3	18.8 ± 0.9	2.4 ± 0.2
		33	17–51	270	-	10	85.3 ± 1.2	34.9 ± 0.8	2.7 ± 0.1

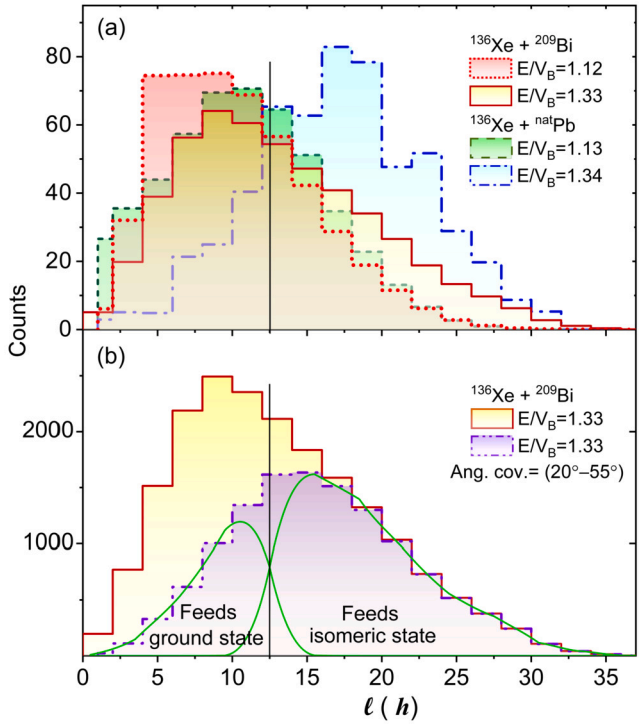

Fig. 3. (a) Spin distribution of ^{211}Po using a dynamical model Langevin approach for ^{136}Xe+ ^{209}Bi at 12% (dotted line) and 33% (solid line) above the Coulomb barrier, and for ^{136}Xe+ ^{nat}Pb at 13% (dashed line) and 34% (dashed-dotted line) above barrier. (b) Unfolding of ^{211}Po into the ground and isomeric states corresponding to 20°-55° of angular coverage of gas cell window. The vertical line indicates the spin value of ^{211m}Po (25/2$^+$).

(or ^{136}Xe+ ^{209}Bi) is significantly larger (or lower) compared to the spin of the ^{211}Po isomer. Variation in the spin distributions considering with and without the angular acceptance of an MNT gas cell can be seen in Fig. 3(b). Feeding of the spin distribution into the ground and isomeric states estimated from equations (1) and (2) is represented with a solid line for the angular acceptance 20°-55° for E/V$_B$ = 1.33.

4. Discussions

The ^{209}Bi target differs from the ^{nat}Pb target in terms of relatively high ground-state spin of ^{209}Bi (9/2$^-$) compared to almost zero spin of ^{nat}Pb (only ^{207}Pb, with 22.1% isotopic abundance, has a non-zero spin 1/2$^-$). The ground-state spin of ^{211}Po has the identical spin as ^{209}Bi but with opposite parity (9/2$^+$). Theory suggests that a larger production of high-spin isomers is more probable in heavy-ion-induced MNT reactions due to the larger angular momentum imparted by projectiles compared to other conventional nuclear reaction processes. This is clearly endorsed by the observed α-spectra in which population of ^{211m}Po, ^{212m}At dominates over corresponding ground states.

The production route of ^{211}Po in the ^{136}Xe+ ^{209}Bi is the 1p1n-transfer channel. However, different feasible production channels of ^{211}Po for the ^{136}Xe+ ^{nat}Pb would be 2p1n, 2p2n, and 2p3n corresponding to the dominant isotopic abundance of ^{208}Pb (52.4%), ^{207}Pb (22.1%), and ^{206}Pb (24.1%). Clearly, the 2p1n channel would be the dominant production route of ^{211}Po. Furthermore, it must be noticed that production of ^{211}Po from the 2p2n and 2p3n channels would not only be suppressed by isotopic abundances but also by the significant reduction of MNT cross-sections with an increasing number of nucleon transfers (20–60%, depending upon the model). Therefore, the combined effect of isotopic abundances and associated reduced cross sections in 1n, 2n, and 3n-transfers in case of ^{nat}Pb would have a similar influence on the spin transfer compared to the 1n-transfer in ^{209}Bi. Hence, 1p-and 2p-transfer will effectively be responsible for any significant variation in the production of ^{211}Po for both reactions and will be further discussed accordingly.

Multiple measurements of α-spectra at different experimental conditions in each run lead to a crucial observation, as shown with open symbols in Fig. 4(a). The IRs of ^{211}Po are independent of various experimental parameters and depend only on the target-projectile combinations (i.e.,^{136}Xe+ ^{209}Bi or ^{136}Xe+ ^{nat}Pb). The final value of the IR was determined by considering the weighted average (WAvg) of the measured IRs, shown with solid symbols. The quantitative deduction of the IRs for ^{211}Po reveals the IR>1, indicating the significant dominance of isomer production over the ground state. It should be stressed here that the IR of ^{211}Po for ^{136}Xe+ ^{nat}Pb is found to be ≈1.8-times higher in comparison to ^{136}Xe+ ^{209}Bi. Possible reasons for the different IR at an incident energy of 945 MeV are: (i) the intrinsic spin of the target, (ii) the angular momentum brought in by the projectile's momentum, and (iii) the number of transferred nucleons. It must be noted that the angular momentum brought in due to the momentum of 945 MeV ^{136}Xe

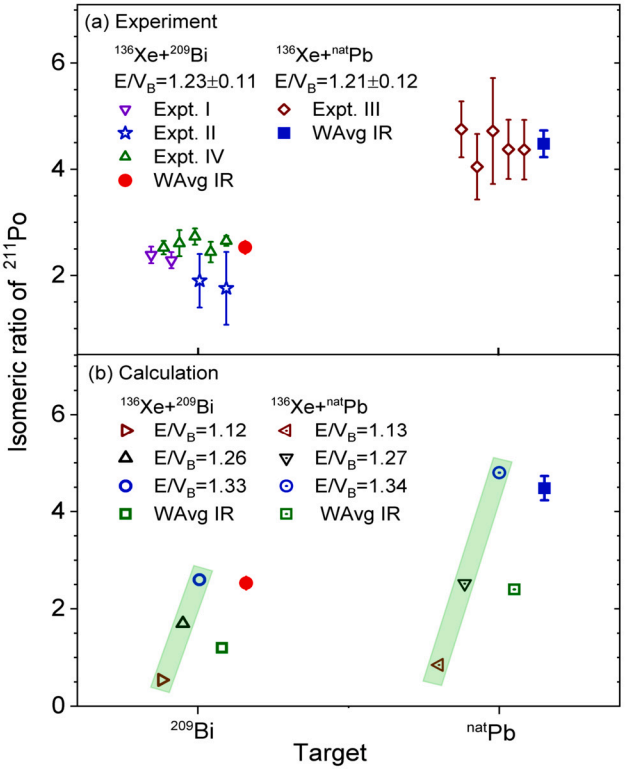

Fig. 4. (a) IRs of ^{211}Po produced in ^{136}Xe+^{209}Bi at E/V$_B$ = 1.23±0.11 and ^{136}Xe+^{nat}Pb at E/V$_B$ = 1.21±0.12 corresponding to 945 MeV beam energy in different experiments. Details of the experimental parameters are described in Table 1. (b) Estimation of IRs of ^{211}Po at three projectile energies and comparison of WAvg of IRs with measured results for ^{136}Xe+^{209}Bi and ^{136}Xe+^{nat}Pb. WAvg refers to the Weighted Average. Strip lines are shown as a guide to the eye for increasing IRs with projectile energy.

beam in the formation of ^{211}Po from both reactions will be identical; however, coupling with the intrinsic spin of different targets could result in different spin values.

A comparison of measured and computed IRs is represented in Fig. 4(b). The theoretical calculation of IRs at 12-13% above the barrier indicates IR<1, which implies the smaller production of isomer compared to the ground state of ^{211}Po. Additionally, the IRs have similar values for both reactions despite the different spin of the targets and production routes. This means that at near-barrier energy, the coupling of the intrinsic spin of ^{209}Bi and the spin brought in via the projectile as well as due to 1*p*-transfer into the ^{209}Bi target is equivalent to the coupling of spin by the projectile as well as the spin due to 2*p*-transfer into the ^{nat}Pb. However, the influence of the target spin on the production of MNT fragments will be more likely to appear at near-barrier energies. This is because of the minimum amount of angular momentum that the projectile brings in, which also results in minimum spin transfer due to the *p*-transfer. This implies a weak dependence of the spin distribution of ^{211}Po on the target spin at near-barrier energy. Therefore, target spin dependence on the spin distribution of an MNT fragment would hardly appear at higher projectile energies.

The calculated IRs shown in Fig. 4(b) were found to increase with increasing projectile energy for both reactions. The increasing nature of the IR can be understood as the projectile energy could bring in more angular momentum to the system via the projectile's momentum as well as the transfer of nucleons (in the case of MNT-induced reactions), indicating a large probability of the population of high-spin states (*i.e.*, isomers, in the present case) of MNT fragments and thereby resulting in higher values of IRs. The optimum angular range of the new gas cells was considered in the theoretical calculation to match the experimental and theoretical scenario. Finally, the weighted average (WAvg) of the

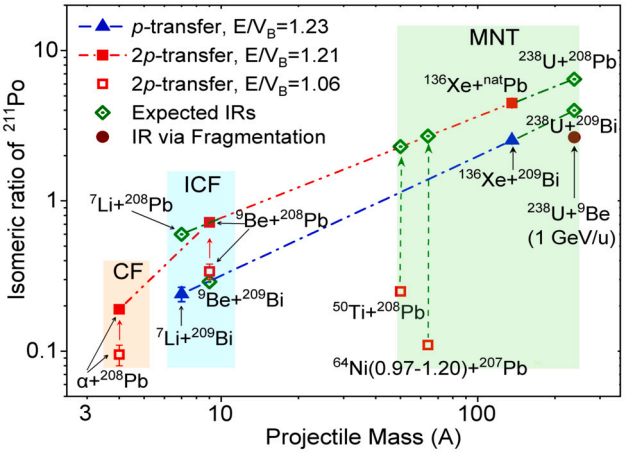

Fig. 5. Comparison of different experimental IRs of ^{211}Po with different projectile masses corresponding to various nuclear reaction processes: α+^{208}Pb [69], ^{7}Li+^{209}Bi and ^{9}Be+^{208}Pb [64], ^{50}Ti+^{208}Pb [70], ^{64}Ni +^{207}Pb [39], ^{136}Xe+^{209}Bi/^{nat}Pb (present work) at 21-23% above the barrier, and ^{238}U+^{9}Be at 1 GeV/u in fragmentation process [71].

estimated IRs was computed to simulate the production of the isomeric (25/2$^+$) and ground (9/2$^+$) states of ^{211}Po for the projectile energy loss within the targets.

It is evident from Fig. 4(b) that the population of the ^{211}Po isomer over the ground state differs for the studied production routes, ^{136}Xe+^{nat}Pb and ^{136}Xe+^{209}Bi. Theoretical calculations (open squares) qualitatively explain the measured values. However, this underpredicts the experimental IRs by a factor of ≈2 for both reactions. Tentative assignment of (25/2$^+$) of ^{211m}Po might be one reason for the quantitative disagreement. The tentative assignment was made using empirical shell-model (ESM) calculations [68]. Moreover, decay of the other two isomeric states (31/2$^-$) and (43/2$^+$) of ^{211}Po (tentatively assigned spin values) might change the independent production of the ground (9/2$^+$) and/or isomeric (25/2$^+$) states, which could result in this inconsistency. Additionally, as discussed in Sec. 3, the angular momentum of TLFs would not be just a sum of the ground-state spin of the target and the angular momentum transferred by projectiles and nucleon transfer. One must also consider the angular momentum carried away by nucleon evaporation from the excited MNT fragments, which would influence the final spin of the product. However, this was not considered in the calculations. More experimental data for different target-projectile systems would be helpful to properly incorporate its contribution in the theoretical calculation. Nonetheless, it is worth concluding that the *p*-transfer channels are strongly correlated with spin distributions and, thereby, the IRs. This means that more *p*-transfer could impart more spin to the MNT fragments and, thereby, more significant production of high-spin state isomers.

Fig. 5 exhibits a comparative study on the IRs of ^{211}Po deduced in the present work together with other experimental results over a wide range of projectile masses. The different shaded regions represent distinct nuclear reaction processes: (i) complete fusion (CF) process in α+^{208}Pb (open square) [69]; (ii) incomplete fusion (ICF) process involved in ^{7}Li +^{209}Bi (solid triangle) and ^{9}Be+^{208}Pb (open square) [64]; and (iii) MNT reaction process using ^{136}Xe+^{nat}Pb (solid square), ^{136}Xe+^{209}Bi (solid triangle) within 21-23% above barrier energies, ^{50}Ti+^{208}Pb and ^{64}Ni+^{207}Pb (open square) at low projectile energies [39,70]; and (iv) via fragmentation reaction process using ^{238}U+^{9}Be at 1 GeV/u (solid circle) [71]. The IR of α+^{208}Pb and ^{9}Be+^{208}Pb at E/V$_B$ = 1.21 (solid square) were extrapolated from the increasing values of IRs reported at lower incident energies; one of them is shown with the open square at E/V$_B$ = 1.06. However, an increment in the IRs and subsequent decrement may be anticipated with increasing projectile energies, similar to other reactions [72,73]. Therefore, the reactions

are essential to validate experimentally. Nonetheless, analysis endorses the increment of IRs populated from the $2p$-channel compared to the $1p$-channel. Anticipated IRs of ^{211}Po for several reactions were shown with an open diamond symbol. The $1p$- and $2p$-transfer channels were indicated with dash-dotted and dash-dot-dot lines, respectively.

The comparative analysis demonstrates that the IRs of ^{211}Po have primarily been affected by two entrance channel parameters: the projectile mass and the transfer channel production route. It is apparent that the IRs of ^{211}Po gradually increase with the projectile mass (see Fig. 5). This reveals the sensitivity of the spin distribution of residues on the projectile mass in different reaction processes. The ICF process is similar to transfer-like processes in which cluster transfer can be favored due to the weakly bound nature of projectiles, like ^{6,7}Li, ^{9}Be [74–76]. In the ICF process, an enhanced angular momentum transfer has been observed in evaporation residues (ERs) compared to CF corresponding to the same production channels; e.g., α-transfer from ^{7}Li in ICF would impart more spin to ER compared to α-particle fusion in CF [64]. Similarly, in the present case, the residue produced from the MNT-induced reaction process via either $1p$- or $2p$-transfer channel can impart more angular momentum to the system than the one formed from the identical transfer of nucleons in the ICF process [64]. This indicates that spin transferred into the target via the transfer of nucleons (sequential or cluster transfer) strongly correlates with the projectile mass. Additionally, the consistent enhancement of IRs for the $2p$-transfer channel compared to the $1p$-transfer channel over an extended mass region in distinct CF, ICF, and MNT reaction processes is worth noticing, which manifests the impact of different p-transfer channels on the spin distributions.

The IRs of ^{211}Po produced from ^{50}Ti+^{208}Pb and ^{64}Ni+^{207}Pb reactions were deduced from the α-spectra at relatively lower projectile energy, $E/V_B = 1.06$ and $E/V_B = 0.21$-1.20, respectively. The experiments were not aimed at the investigation of IRs [39,70]. Significantly lower values of the IR were found for both reactions shown in Fig. 5. This might be due to either lower projectile energy or limited angular coverage of the experimental setup ($0° \pm 2°$), or both [64,77]. The trend line obtained from the IRs of ^{211}Po from ICF and MNT processes predicts the large value of IRs for ^{50}Ti and ^{64}Ni projectiles at $E/V_B = 1.21$. Moreover, the IRs from ^{238}U+^{209}Bi/^{nat}Pb are predicted to be large compared to one obtained from ^{238}U+^{9}Be via fragmentation process. Hence, the comparative analysis provides a strong impetus to investigate the IRs for different target-projectile combinations populating ^{211}Po, including MNT reactions: ^{50}Ti+^{208}Pb, ^{64}Ni+^{207}Pb, and ^{238}U+^{208}Pb/^{209}Bi. Examining these reactions at near-barrier energies is crucial for paving a path toward a limpid understanding of spin distributions. Consequently, exploring the ^{238}U+^{209}Bi/^{208}Pb/^{238}U reactions via the MNT approach is one of the prime objectives of an approved proposal to be performed soon at FRS-IC, GSI [49,78].

5. Summary

First measurement on the IRs of ^{211}Po was accomplished from the α-decay spectra produced via different channels of MNT reactions using ^{136}Xe+^{209}Bi and ^{136}Xe+^{nat}Pb. The population of isomers over the corresponding ground states was dominantly observed in different measurements of α-spectra. A dynamical approach based on Langevin equations was utilized to compute spin distributions of the MNT fragment for the first time and subsequently estimate the IRs at three distinct energies for both reactions. Close agreement between the computed IRs of ^{211}Po from ^{136}Xe+^{209}Bi and ^{136}Xe+^{nat}Pb reactions at near-barrier energy indicate a weak dependence of target spin on the spin distribution and thereby would hardly affect the IRs at high energies, *i.e.*, 26-34% above the barrier. Deduced IRs of ^{211}Po from ^{136}Xe+^{nat}Pb has been found to be increased by a factor of ≈1.8-times than obtained from ^{136}Xe+^{209}Bi. The considerable increment in the ^{211}Po isomer can be attributed to the production route of the $2p$-transfer channel in ^{136}Xe+^{nat}Pb compared to the $1p$-transfer channel in ^{136}Xe+^{209}Bi. The estimated IRs were found to be strongly affected by projectile energy and qualitatively consistent with experimental findings of both reactions. However, theoretical estimations were underestimated by a factor of two compared to the measured IRs.

Comparative analysis on the IRs of ^{211}Po over the projectile mass in different nuclear reaction processes at $E/V_B \approx 1.21$-1.23 reveals two main entrance channel parameters: projectile mass and transfer channel production route, which strongly affect the IRs and, thereby, would play a major role in the spin distributions. The angular momentum transferred into the target via nucleon transfer over the identical channels is found to increase with the projectile mass. The IRs of ^{211}Po have been found to be enhanced for the $2p$-channel than for the $1p$-channel over an extended mass range of the projectiles, inducing via CF, ICF, and MNT reaction processes. Present experimental and theoretical findings invoke for the comprehensive and systematic works to validate the predicted IRs for ^{9}Be+^{209}Bi, ^{7}Li+^{208}Pb, ^{50}Ti/^{64}Ni+^{208}Pb, ^{238}U+^{208}Pb/^{209}Bi including many other feasible target-projectile systems above Coulomb barrier energies.

Declaration of competing interest

The authors declare that they have no known competing financial interests or personal relationships that could have appeared to influence the work reported in this paper.

Data availability

All the relevant data described in the manuscript is already reported in the Table.

Acknowledgements

The author would like to express his sincere and deep sense of indebtedness to Dr. A.V. Karpov and Dr. V.V. Saiko for their unconditional continuous support in the theoretical estimation works. We thank the cyclotron team for their efforts to provide a stable beam condition. The work was financially supported by the EU Horizon 2020 research and innovation program (ERC Consolidator Grant 2017) under Grant Agreement No. 771036, 861198–LISA–H2020-MSCA-ITN-2019, and from DAAD Grant No. 57610603. Zs.P. acknowledges support by the Science and Technology Facilities Council (STFC). P.C. acknowledges contract PN 23.21.01.06 of the Romanian Ministry of Research and Innovation. I.M. acknowledges partial support by The Israel Science Foundation, Grant No. 2575/21.

References

[1] T. Otsuka, A. Gade, O. Sorlin, T. Suzuki, Y. Utsuno, Evolution of shell structure in exotic nuclei, Rev. Mod. Phys. 92 (2020) 015002, https://doi.org/10.1103/RevModPhys.92.015002.

[2] C.J. Horowitz, A. Arcones, B. Côté, I. Dillmann, W. Nazarewicz, I.U. Roederer, H. Schatz, A. Aprahamian, D. Atanasov, A. Bauswein, et al., r-process nucleosynthesis: connecting rare-isotope beam facilities with the cosmos, J. Phys. G, Nucl. Part. Phys. 46 (2019) 083001, https://doi.org/10.1088/1361-6471/ab0849.

[3] S. Heinz, H.M. Devaraja, Nucleosynthesis in multinucleon transfer reactions, Eur. Phys. J. A 58 (2022) 114, https://doi.org/10.1140/epja/s10050-022-00771-1.

[4] G. Wendell Misch, Surja K. Ghorui, Projjwal Banerjee, Yang Sun, Matthew R. Mumpower, Astromers: nuclear isomers in astrophysics, Astrophys. J. Suppl. Ser. 252 (1) (2021) 2, https://doi.org/10.3847/1538-4365/abc41d.

[5] A. Aprahamian, Y. Sun, Long live isomer research, Nat. Phys. 1 (2005) 81, https://www.nature.com/articles/nphys150.pdf.

[6] O. Kaleja, B. Anđelic, O. Bezrodnova, et al., Direct high-precision mass spectrometry of superheavy elements with SHIPTRAP, Phys. Rev. C 106 (2022) 054325, https://journals.aps.org/prc/pdf/10.1103/PhysRevC.106.054325.

[7] P. Jachimowicz, M. Kowal, J. Skalski, Hindered α decays of heaviest high-K isomers, Phys. Rev. C 98 (2018) 014320, https://journals.aps.org/prc/pdf/10.1103/PhysRevC.98.014320.

[8] D. Kumar, M. Maiti, R. Prajapat, A. Chauhan, R. Biswas, J. Gehlot, S. Nath, R. Kumar, N. Madhavan, G. Naga Jyothi, R.N. Sahoo, Md. Moin Shaikh, V. Srivastava, Analysis of mass-separated evaporation residues formed in 32S+70,68Zn fusion reactions:

the special case of 97,95Ru, Phys. Rev. C 104 (2021) 014602, https://doi.org/10.1103/PhysRevC.104.014602.

[9] M. Maiti, S. Lahiri, D. Kumar, D. Choudhury, Separation of no-carrier-added astatine radionuclides from alpha-particle irradiated lead-bismuth eutectic target: a classical method, Appl. Radiat. Isot. 127 (2017) 227, https://doi.org/10.1016/j.apradiso.2017.06.020.

[10] D. Kumar, M. Maiti, S. Lahiri, Production of no-carrier-added 97Ru from 11B-activated natural yttrium target and its subsequent separation using liquid–liquid extraction, Sep. Sci. Technol. 52 (2017) 2372, https://doi.org/10.1080/01496395.2017.1279179.

[11] D. Kumar, M. Maiti, D. Choudhury, S. Lahiri, Production yield of residues in 11B+93Nb reaction and separation of trace scale Pd from bulk Nb using liquid-liquid extraction, Sep. Sci. Technol. 54 (2019) 1661, https://doi.org/10.1080/01496395.2019.1565778.

[12] P.M. Walker, G.D. Dracoulis, Energy traps in atomic nuclei, Nature 399 (1999) 35, https://doi.org/10.1038/19911.

[13] The European Physical Journal Special Topics: Nuclear Isomers, https://epjst.epj.org/component/toc/?task=topic%26id=1992.

[14] L. Zhu, Jun Su, C. Li, Feng-Shou Zhang, How to approach the island of stability: reactions using multinucleon transfer or radioactive neutron-rich beams?, Phys. Lett. B 829 (2022) 137113, https://doi.org/10.1016/j.physletb.2022.137113.

[15] D. Kumar et al., Mass measurements for the MNT reaction ^{136}Xe on ^{176}Yb at IGISOL, Proposal to PAC-JYFL, September 2021, No. I287.

[16] R.M. Pérez-Vidal, F. Galtarossa, T. Mijatović, S. Szilner, I. Zanon, D. Brugnara, J. Pellumaj, M. Ciemala, J.J. Valiente-Dobón, L. Corradi, E. Clément, S. Leoni, B. Fornal, M. Siciliano, A. Gadea, Nuclear structure advancements with multi-nucleon transfer reactions, Eur. Phys. J. A 59 (2023) 114, https://doi.org/10.1140/epja/s10050-023-01027-2.

[17] D. Kumar, E.M. Kozulin, G.N. Knyazheva, et al., Investigation on competing fission modes in 178Pt* produced by 36Ar + 142Nd reaction up to high excitation energies, Bull. Russ. Acad. Sci., Phys. 85 (12) (2021) 1479, https://doi.org/10.3103/S1062873821120194.

[18] K.V. Novikov, E.M. Kozulin, G.N. Knyazheva, et al., Investigation of fusion probabilities in the reactions with 52, 54Cr, 64Ni, and 68Zn ions leading to the formation of Z=120 superheavy composite systems, Phys. Rev. C 102 (2020) 044605, https://doi.org/10.1103/PhysRevC.102.044605.

[19] E.M. Kozulin, A.A. Bogachev, G.N. Knyazheva, V.V. Saiko, I.M. Itkis, K.V. Novikov, D. Kumar, P.P. Singh, Exclusive mass-energy distributions of the fast fission fragments in the 40Ca+144Sm reaction, Phys. At. Nucl. 86 (2023) 56–69, https://doi.org/10.1134/S1063778823020126.

[20] D. Kumar, E.M. Kozulin, M. Cheralu, et al., Study of mass-asymmetric fission of 180,190Hg formed in the 36Ar + 144,154Sm reactions, Bull. Russ. Acad. Sci., Phys. 84 (2020) 1001, https://doi.org/10.3103/S1062873820080213.

[21] V.I. Zagrebaev, W. Greiner, Production of new heavy isotopes in low-energy multinucleon transfer reactions, Phys. Rev. Lett. 101 (2008) 122701, https://doi.org/10.1103/PhysRevLett.101.122701.

[22] A.V. Karpov, V.V. Saiko, Modeling near-barrier collisions of heavy ions based on a Langevin-type approach, Phys. Rev. C 96 (2017) 024618, https://doi.org/10.1103/PhysRevC.96.024618.

[23] V.V. Saiko, A.V. Karpov, Analysis of multinucleon transfer reactions with spherical and statically deformed nuclei using a Langevin-type approach, Phys. Rev. C 99 (2019) 014613, https://doi.org/10.1103/PhysRevC.99.014613.

[24] V.V. Saiko, A.V. Karpov, Multinucleon transfer as a method for production of new heavy neutron-enriched isotopes of transuranium elements, Eur. Phys. J. A 58 (2022) 41, https://doi.org/10.1140/epja/s10050-022-00688-9.

[25] C. Li, F. Zhang, J. Li, L. Zhu, J. Tian, N. Wang, F.S. Zhang, Multinucleon transfer in the 136Xe+208Pb reaction, Phys. Rev. C 93 (2016) 014618, https://doi.org/10.1103/PhysRevC.93.014618.

[26] C. Li, P. Wen, J. Li, G. Zhang, B. Li, X. Xu, Z. Liu, S. Zhu, F.S. Zhang, Production mechanism of new neutron-rich heavy nuclei in the 136Xe+198Pt reaction, Phys. Lett. B 776 (2018) 278, https://doi.org/10.1016/j.physletb.2017.11.060.

[27] C. Li, J. Tian, F.S. Zhang, Production mechanism of the neutron-rich nuclei in multinucleon transfer reactions: a reaction time scale analysis in energy dissipation process, Phys. Lett. B 809 (2020) 135697, https://doi.org/10.1016/j.physletb.2020.135697.

[28] L. Zhu, Shell inhibition on production of N = 126 isotones in multinucleon transfer reactions, Phys. Lett. B 816 (2021) 136226, https://doi.org/10.1016/j.physletb.2021.136226.

[29] K. Zhao, Z. Liu, F.S. Zhang, N. Wang, Production of neutron-rich N = 126 nuclei in multinucleon transfer reactions: comparison between 136Xe + 198Pt and 238U + 198Pt reactions, Phys. Lett. B 815 (2021) 136101, https://doi.org/10.1016/j.physletb.2021.136101.

[30] E.M. Kozulin, E. Vardaci, G.N. Knyazheva, et al., Mass distributions of the system 136Xe+208Pb at laboratory energies around the Coulomb barrier: a candidate reaction for the production of neutron-rich nuclei at N=126, Phys. Rev. C 86 (2012) 044611, https://doi.org/10.1103/PhysRevC.86.044611.

[31] Y.X. Watanabe, Y.H. Kim, S.C. Jeong, et al., Pathway for the production of neutron-rich isotopes around the N=126 shell closure, Phys. Rev. Lett. 115 (2015) 172503, https://doi.org/10.1103/PhysRevLett.115.172503.

[32] A. Utepov, D. Ackermann, C. Stodel, et al., Multinucleon transfer reactions in the 238U + 238U system studied with the VAMOS+AGATA+ID-fix*, Acta Phys. Pol. B, Proc. Suppl. 16 (2023) 4–A11, https://doi.org/10.5506/APhysPolBSupp.16.4-A11.

[33] Y. Son, Y.H. Kim, Y. Cho, et al., CATLIFE (complementary arm for target LIke FragmEnts): spectrometer for target like fragments at VAMOS++, Nucl. Instrum. Methods Phys. Res., Sect. B 540 (2023) 234, https://doi.org/10.1016/j.nimb.2023.04.024.

[34] E. Clément, C. Michelagnoli, G. de France, et al., Conceptual design of the AGATA 1π array at GANIL, Nucl. Instrum. Methods Phys. Res., Sect. A 855 (2017) 1, https://doi.org/10.1016/j.nima.2017.02.063.

[35] T. Welsh, W. Loveland, R. Yanez, et al., Modeling multi-nucleon transfer in symmetric collisions of massive nuclei, Phys. Lett. B 771 (2017) 119, https://doi.org/10.1016/j.physletb.2017.05.044.

[36] V.V. Desai, W. Loveland, R. Yanez, G. Lane, S. Zhu, A.D. Ayangekaa, J.P. Greene, F.G. Kondev, R.V.F. Janssens, P.A. Copp, The reaction: a detailed re-examination, Eur. Phys. J. A 56 (2020) 150, https://doi.org/10.1140/epja/s10050-020-00154-4.

[37] V.V. Desai, A. Pica, W. Loveland, et al., Multinucleon transfer in the interaction of 977 MeV and 1143 MeV 204Hg with 208Pb, Phys. Rev. C 101 (2020) 034612, https://doi.org/10.1103/PhysRevC.101.034612.

[38] J.S. Barrett, W. Loveland, R. Yanez, et al., 136Xe + 208Pb reaction: a test of models of multinucleon transfer reactions, Phys. Rev. C 91 (2015) 064615, https://doi.org/10.1103/PhysRevC.91.064615.

[39] V.F. Comas, S. Hofmann, D. Ackermann, J.A. Heredia, F.P. Heßberger, J. Khuyagbaatar, B. Kindler, B. Lommel, R. Mann, Study of multi-nucleon transfer reactions in 58, 64Ni + 207Pb collisions at the velocity filter SHIP, Eur. Phys. J. A 49 (2013) 112, https://doi.org/10.1140/epja/i2013-13112-x.

[40] W. Królas, R. Broda, B. Fornal, T. Pawłat, H. Grawe, K.H. Maier, M. Schramm, R. Schubart, et al., Gamma coincidence study of 208Pb+350 MeV 64Ni collisions, Nucl. Phys. A 724 (2003) 289, https://doi.org/10.1016/S0375-9474(03)01544-6.

[41] A. Gadea, D.R. Napoli, G. de Angelis, et al., Coupling a CLOVER detector array with the PRISMA magnetic spectrometer, Eur. Phys. J. A 20 (2004) 193, https://doi.org/10.1140/epja/i2002-10352-9.

[42] A. Vogt, B. Birkenbach, P. Reiter, et al., Light and heavy transfer products in 136Xe + 238U multinucleon transfer reactions, Phys. Rev. C 92 (2015) 024619, https://doi.org/10.1103/PhysRevC.92.024619.

[43] J.J. Valiente-Dobón, R. Menegazzo, A. Goasduff, et al., Conceptual design of the AGATA 2π array at LNL, Nucl. Instrum. Methods Phys. Res., Sect. A 1049 (2023) 168040, https://doi.org/10.1016/j.nima.2023.168040.

[44] S. Koulouris, G.A. Souliotis, F. Cappuzzello, et al., Multinucleon transfer channels from 70Zn(15 MeV/nucleon) + 64Ni collisions, Phys. Rev. C 108 (2023) 044612, https://doi.org/10.1103/PhysRevC.108.044612.

[45] F. Cappuzzello, C. Agodi, D. Carbone, et al., The MAGNEX spectrometer: results and perspectives, Eur. Phys. J. A 52 (2016) 167, https://doi.org/10.1140/epja/i2016-16167-1.

[46] K. Hirose, K. Nishio, S. Tanaka, et al., Role of multichance fission in the description of fission-fragment mass distributions at high energies, Phys. Rev. Lett. 119 (2017) 222501, https://doi.org/10.1103/PhysRevLett.119.222501.

[47] W. Loveland, Synthesis of transactinide nuclei using radioactive beams, Phys. Rev. C 76 (2007) 014612, https://doi.org/10.1103/PhysRevC.76.014612.

[48] P.H. Chen, F. Niu, W. Zuo, Z.Q. Feng, Approaching the neutron-rich heavy and superheavy nuclei by multinucleon transfer reactions with radioactive isotopes, Phys. Rev. C 101 (2020) 024610, https://doi.org/10.1103/PhysRevC.101.024610.

[49] T. Dickel, A. Kankainen, A. Spătaru, et al., Multi-nucleon transfer reactions at ion catcher facilities - a new way to produce and study heavy neutron-rich nuclei, J. Phys. Conf. Ser. 1668 (2020) 012012, https://doi.org/10.1088/1742-6596/1668/1/012012, https://doi.org/10.1103/PhysRevResearch.5.L022021.

[50] A. Zadvornaya, et al., Commissioning of a multinucleon-transfer gas cell at the IGISOL facility, to be published.

[51] A. Spătaru, D.L. Balabanski, O. Beliuskina, et al., Production of exotic nuclei via MNT reactions using gas cells, Acta Phys. Pol. B 51 (2020) 817, https://doi.org/10.5506/APhysPolB.51.817.

[52] A. Rotaru, D. Amanbayev, D.L. Balabanski, et al., INCREASE: an in-cell reaction system for multi-nucleon transfer and spontaneous fission at the FRS ion catcher, Nucl. Instrum. Methods Phys. Res., Sect. B 512 (2022) 83, https://doi.org/10.1016/j.nimb.2021.11.018.

[53] G. Savard, M. Brodeur, J.A. Clark, R.A. Knaack, A.A. Valverde, The N = 126 factory: a new facility to produce very heavy neutron-rich isotopes, Nucl. Instrum. Methods Phys. Res., Sect. B 463 (2020) 258, https://doi.org/10.1016/j.nimb.2019.05.024.

[54] J. Even, X. Chen, A. Soylu, et al., The NEXT project: towards production and investigation of neutron-rich heavy nuclides, Atoms 10 (2022) 59, https://doi.org/10.3390/atoms10020059.

[55] T. Niwase, Y.X. Watanabe, Y. Hirayama, et al., Discovery of new isotope 241U and systematic high-precision atomic mass measurements of neutron-rich Pa-Pu nuclei produced via multinucleon transfer reactions, Phys. Rev. Lett. 130 (2023) 132502, https://doi.org/10.1103/PhysRevLett.130.132502.

[56] Y. Hirayama, Y.X. Watanabe, M. Mukai, et al., β- and γ-decay spectroscopy of 197,198Os, Phys. Rev. C 98 (2018) 014321, https://doi.org/10.1103/PhysRevC.98.014321.

[57] H. Choi, Y. Hirayama, S. Choi, et al., In-gas-cell laser ionization spectroscopy of 194,196Os isotopes by using a multireflection time-of-flight mass spectrograph, Phys. Rev. C 102 (2020) 034309, https://doi.org/10.1103/PhysRevC.102.034309.

[58] Y. Hirayama, Y.X. Watanabe, M. Mukai, et al., Doughnut-shaped gas cell for KEK isotope separation system, Nucl. Instrum. Methods Phys. Res., Sect. B 412 (2017) 11, https://doi.org/10.1016/j.nimb.2017.08.037.

[59] M. Mukai, Y. Hirayama, Y.X. Watanabe, et al., In-gas-cell laser resonance ionization spectroscopy of 196,197,198Ir, Phys. Rev. C 102 (2020) 054307, https://doi.org/10.1103/PhysRevC.102.054307.

[60] J. Ärje, J. Äystö, H. Hyvönen, P. Taskinen, V. Koponen, J. Honkanen, K. Valli, The ion guide isotope separator on-line, IGISOL, Nucl. Instrum. Methods Phys. Res., Sect. A 247 (1986) 431, https://doi.org/10.1016/0168-9002(86)90404-3.

[61] I. Moore, T. Eronen, D. Gorelov, et al., Towards commissioning the new IGISOL-4 facility, Nucl. Instrum. Methods Phys. Res., Sect. B 317 (2013) 208, https://doi.org/10.1016/j.nimb.2013.06.036.

[62] J.F. Ziegler, M.D. Ziegler, J.P. Biersack, SRIM – the stopping and range of ions in matter (2010), Nucl. Instrum. Methods Phys. Res., Sect. B 268 (2010) 1818, https://doi.org/10.1016/j.nimb.2010.02.091.

[63] P. Karvonen, I.D. Moore, T. Sonoda, T. Kessler, H. Penttilä, K. Peräjärvi, P. Ronkanen, J. Äystö, A sextupole ion beam guide to improve the efficiency and beam quality at IGISOL, Nucl. Instrum. Methods Phys. Res., Sect. B 266 (2008) 4794, https://doi.org/10.1016/j.nimb.2008.07.022.

[64] L.R. Gasques, M. Dasgupta, D.J. Hinde, T. Peatey, A. Diaz-Torres, J.O. Newton, Isomer ratio measurements as a probe of the dynamics of breakup and incomplete fusion, Phys. Rev. C 74 (2006) 064615, https://doi.org/10.1103/PhysRevC.74.064615.

[65] G. Häfner, K. Moschner, A. Blazhev, et al., Properties of γ-decaying isomers in the 100Sn region populated in fragmentation of a 124Xe beam, Phys. Rev. C 100 (2019) 024302, https://doi.org/10.1103/PhysRevC.100.024302.

[66] S. Pal, R. Palit, Angular momentum population in fragmentation reactions, Phys. Lett. B 665 (2008) 164, https://doi.org/10.1016/j.physletb.2008.06.040.

[67] A.V. Karpov, V.V. Saiko, Calculation of the isomeric ratio of ^{211}Po for ^{136}Xe+ ^{209}Bi/^{nat}Pb, private communication.

[68] T.R. McGoram, G.D. Dracoulis, A.P. Byrne, A.R. Poletti, S. Bayer, High-spin isomers in 211Po and related structures in 210Po and 212Po, Nucl. Phys. A 637 (1998) 469, https://doi.org/10.1016/S0375-9474(98)00227-9.

[69] A.R. Barnett, J.S. Lilley, Interaction of alpha particles in the lead region near the Coulomb barrier, Phys. Rev. C 9 (1974) 2010, https://doi.org/10.1103/PhysRevC.9.2010.

[70] H.M. Devaraja, A.V. Yeremin, S. Heinz, A.G. Popeko, The study of multi-nucleon transfer reactions for synthesis of new heavy and superheavy nuclei, Phys. Part. Nucl. Lett. 693 (2022) 19, https://doi.org/10.1134/S1547477122060085.

[71] T. Dickel, W.R. Plaß, S. Ayet San Andres, et al., First spatial separation of a heavy ion isomeric beam with a multiple-reflection time-of-flight mass spectrometer, Phys. Lett. B 137 (2015) 744, https://doi.org/10.1016/j.physletb.2015.03.047.

[72] D. Kumar, M. Maiti, S. Lahiri, New measurement of residual cross sections from Nb reaction: a comparative study of PEQ models and nuclear level densities, Eur. Phys. J. Plus 135 (2020) 176, https://doi.org/10.1140/epjp/s13360-020-00152-x.

[73] R. Prajapat, M. Maiti, D. Kumar, Fusion-fission events in the 11B+181Ta reaction up to 5.7 MeV/nucleon energy, Phys. Rev. C 103 (2021) 014608, https://doi.org/10.1103/PhysRevC.103.014608.

[74] D. Kumar, M. Maiti, S. Lahiri, Li-induced reaction on natMo: a study of complete versus incomplete fusion, Phys. Rev. C 96 (2017) 014617, https://doi.org/10.1103/PhysRevC.96.014617.

[75] R. Prajapat, M. Maiti, Probing the influence of incomplete fusion in the 6Li+89Y reaction up to 7.2 MeV/nucleon energy, Phys. Rev. C 103 (2021) 034620, https://doi.org/10.1103/PhysRevC.103.034620.

[76] D. Kumar, M. Maiti, Incomplete fusion analysis of the 7Li-induced reaction on 93Nb within 3–6.5 MeV/nucleon, Phys. Rev. C 96 (2017) 044624, https://doi.org/10.1103/PhysRevC.96.044624.

[77] Z. Liao, L. Zhu, Z. Gao, J. Su, C. Liet, Optimal detection angles for producing N = 126 neutron-rich isotones in multinucleon transfer reactions, Phys. Rev. Res. 5 (2023) L022021, https://doi.org/10.1103/PhysRevResearch.5.L022021.

[78] T. Dickel, et al., Proposal to G-PAC 2018/2019, No. S475 379.